

Department of Chemistry, McGill University,  
and Pulp and Paper Research Institute of Canada, Montreal (Canada)

## A rigorous theory of ring tensiometry

C. Hub and S. G. Mason

With 10 figures and 6 tables

(Received April 15, 1974)

### List of symbols

$a$	= radius of the ring wire; $\bar{a} \equiv a/\sqrt{C_{23}}$ .
$A_i$	= quantity defined by [13a].
$b$	= radius of curvature at $r = 0$ of the inner meniscus.
$C_{23}$	= $(\rho_2 - \rho_3)g/\gamma_{23}$ .
$f$	= Harkins-Jordan factor.
$F$	= maximum equilibrium force of detachment.
$g$	= gravity.
$h$	= height of the ring; $\bar{h} \equiv h/\sqrt{C_{23}}$ .
$r_i$	= $r$ -coordinate of the $i$ meniscus; $\bar{r}_i \equiv r_i/\sqrt{C_{23}}$ .
$R$	= radius of the ring; $\bar{R} \equiv R/\sqrt{C_{23}}$ .
$v$	= volume of the liquid raised; $\bar{v} \equiv v C_{23}^{3/2}$ .
$V$	= maximum $v$ ; $\bar{V} \equiv V C_{23}^{3/2}$ .
$z_0$	= height of the inner meniscus at $r = 0$ , $\bar{z}_0 \equiv z_0/\sqrt{C_{23}}$ .
$z_i$	= $z$ -coordinate of the $i$ meniscus, $\bar{z}_i \equiv z_i/\sqrt{C_{23}}$ .

### Greek

$\beta_i$	= shape parameter of the $i$ meniscus.
$\gamma_{23}$	= interfacial tension (23 interface).
$\lambda_i$	= a quantity defined by [12].
$\rho_i$	= density of the phase $i$ .
$\phi_i$	= slope angle of the $i$ meniscus profile.
$\psi_i$	= angle between the lines drawn from the center of the ring wire, vertically downwards and to the $i$ contact line.

### Notes:

1. The subscript  $c$  denotes values at the contact line.
2. A bar over a symbol designates a dimensionless quantity.
3.  $i = 1$  refers to the inner meniscus;  $i = 2$ , the outer meniscus.

### Introduction

Of the many methods of measuring the surface and interfacial tension of liquids, that based on the ring tensiometer is probably the most widely used. By measuring the maximum equilibrium force  $F$  required to detach a

circular ring from a liquid surface, the surface tension  $\gamma_{23}$  can be determined using the relation

$$\gamma_{23} = \frac{F}{4\pi R} f\left(\frac{R^3}{V}, \frac{R}{a}\right). \quad [1]$$

$R$  and  $a$  are the respective radii of the ring and the wire (fig. 1). The dimensionless quantity  $f$  is the Harkins and Jordan factor (1) which allows for the thickness of the wire and which is unity in the limit  $a = 0$  and  $R \rightarrow \infty$ ; it is a function of the dimensionless parameters  $R^3/V$  and  $R/a$ , where  $V$  is the volume of the liquid raised above the flat level of the liquid surface when the maximum (or critical) force  $F$  is reached. At mechanical equilibrium,  $F = (\rho_2 - \rho_3)gV$ , where  $\rho_2$  is the density of the liquid,  $\rho_3$  is the density of the fluid (a gas or another liquid) above the liquid, and  $g$  is gravity. If  $v$  is the volume of the liquid raised as the ring is gradually displaced vertically,  $V$  is therefore the largest equilibrium  $v$  attainable. As the ring is raised beyond this critical state,  $v$  begins to decrease and the ring detaches from the liquid surface.

Values of  $f$  were determined experimentally by Harkins and Jordan (1) to embrace an extensive range of  $\gamma_{23}$ . Freud and Freud (2) subsequently calculated  $f$  theoretically and found good agreement with the Harkins-Jordan numerical values and thereby made the ring method absolute. The Harkins-Jordan tabulations of  $f$  are available for the ranges,  $R^3/V = 0.3$  to 3.5 and  $R/a = 30$  to 80. Extensions of these ranges have been made in order to use the method in liquid/liquid systems, up to  $R^3/V = 7.5$  for systems with low  $\gamma_{23}$  but with a large density difference

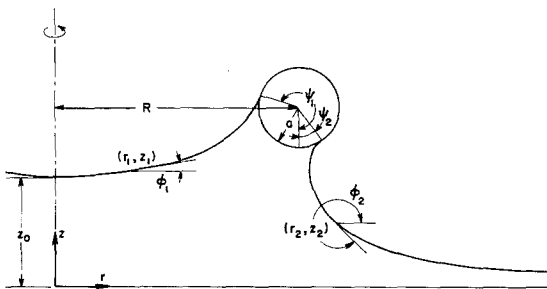


Fig. 1. A half section of a circular ring and the inner and outer menisci attached to it

across the interface (3), and down to 0.045 for systems with large  $\gamma_{23}$  but with a small density difference (4); these extensions were made by extrapolating the Harkins-Jordan values, and were supported by limited experimental measurements.

The main purpose of the present study is to extend the range of the theoretical values of  $f$ . In our analysis, we make use of our general theory (5) of the stability of axisymmetric particles at liquid interfaces in which the method of identifying the characteristic equilibrium states of a solid body at liquid interfaces is given. The method permits accurate and efficient calculations of the factor  $f$  for a wider range of parameter values than the

previous methods. The theoretical calculations also provide us with interesting supplementary information, some of which can be used to increase the accuracy of the ring method.

The rigorous theoretical treatment presented here reaffirms the meaning of the maximum equilibrium force  $F$  measured, which Harkins and Jordan precisely defined but still appears to be misunderstood (6). It is not the force immediately before the ring detaches from the fluid interface; the ring may be displaced beyond the position of maximum force  $F$  while still in equilibrium, until a second position is reached at which the inner and outer menisci approach one another so closely that the thin film intervening them ruptures. An example of how the pulling force changes as the ring is displaced vertically, is shown in fig. 2, where equilibrium is maintained beyond the position of the maximum force  $F$ . Similar behavior of a sphere displaced through an interface has been predicted and observed (7).

We also examine the validity of the approximation that, if the radius of the ring is large compared to the dimensions of the menisci, the ring may be considered as a straight circular cylinder using the theoretical treatment of Princen and Mason (8). Cram and

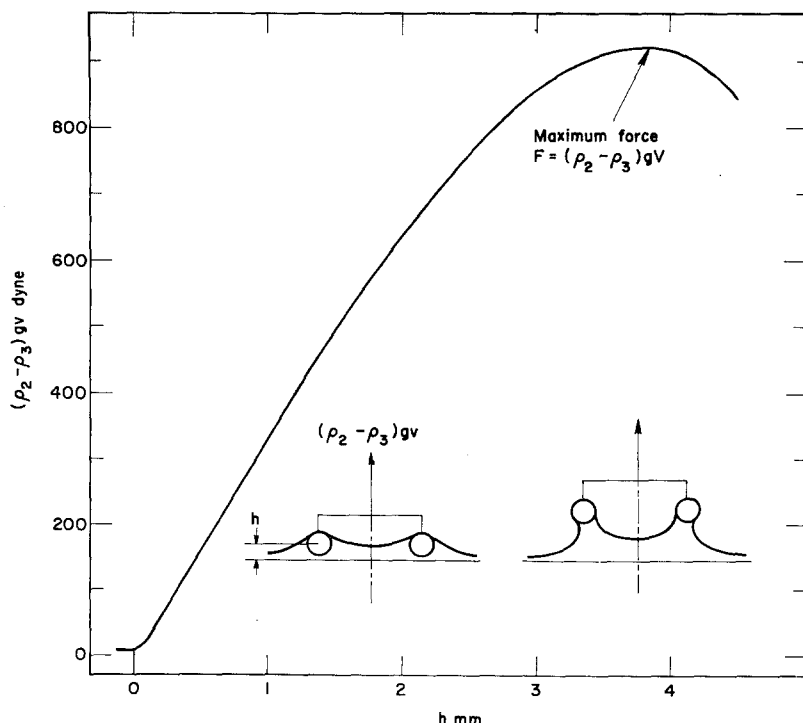


Fig. 2. A typical measured force-displacement curve, for the air/water interface ( $R/a = 53.9$ ;  $2\pi R = 6.020$  cm;  $\rho_2 - \rho_3 = 1.0$  gr/ml;  $R^3/V = 0.940$ ;  $\gamma_{23} = 71.9$  dyne/cm)

*Haynes* (9), using the approximation, studied the effect of the finite contact angle the fluid menisci make with the ring surface. As shown in Section IV, this approximation proves to be a poor one unless corrections are made for the azimuthal curvature of the ring.

To treat the problem theoretically in the simplest mathematical form, we use the following dimensionless variables combining various physical parameters:

$$\bar{R} \equiv R\sqrt{C_{23}}, \bar{a} \equiv a\sqrt{C_{23}}, \bar{V} \equiv V C_{23}^{3/2} \text{ and} \\ \bar{v} \equiv v C_{23}^{-1/2}$$

where

$$C_{23} \equiv (\varrho_2 - \varrho_3) g / \gamma_{23},$$

$\sqrt{2/C_{23}}$  being the conventional capillary constant (10). The factor  $f$  is then expressed as a function of  $\bar{R}^3/\bar{V} \equiv R^3/V$  and  $\bar{R}/\bar{a} \equiv R/a$ :

$$f\left(\frac{\bar{R}^3}{\bar{V}}, \frac{\bar{R}}{\bar{a}}\right) = \frac{4\pi\bar{R}}{\bar{V}}. \quad [1a]$$

To determine theoretically the maximum  $\bar{v}$  ( $= \bar{V}$ ) as a function of  $\bar{R}$  and  $\bar{a}$ , we must calculate  $\bar{v}$  as the dimensionless height of the ring center,  $\bar{h} \equiv h\sqrt{C_{23}}$ , is gradually increased. This requires the equilibrium shapes of the inner and outer menisci attached to the ring. Since this can only be done by numerical means (11, 12), the theoretical calculation of the correction factors for the entire useful range of  $R^3/V$  with meaningful accuracy demands prohibitive time and effort. This difficulty can be partly resolved by deriving analytically the condition at the state of the maximum volume, as described in the next Section. The volume  $\bar{v}$  then need not be calculated at every position of the ring as it is displaced, thus leading to a substantial reduction in the numerical calculations.

In Section II, we first describe the conditions for mechanical equilibrium of a ring at a fluid interface, and then derive the condition necessary to attain the maximum volume  $\bar{V}$ . In Section III, we calculate  $\bar{V}$  for a ring of given  $\bar{R}$  and  $\bar{a}$ , and then the factor  $f$  for the range of  $R^3/V = 0.025$  to 20.0 and  $R/a = 30$  to 80. We also present, as functions of  $R^3/V$  and  $R/a$ , the shape parameters which identify the shapes of the inner and outer menisci attached to the ring at the critical state and the locations of the

inner and outer contact lines on the surface of the ring wire in the critical state. To avoid the possibility that the ring detaches before reaching  $\bar{V}$  because of instability of the menisci or the rupture of the thin film, we calculate and compare  $\bar{v}$  and  $\bar{h}$  for given  $\bar{R}$  and  $\bar{a}$ , (i) when  $\bar{V}$  is attained; (ii) when the maximum equilibrium  $\bar{h}$  is attained; (iii) when the inner and outer menisci come into contact with each other. To construct the tables of  $f$  for the region  $R^3/V > 5.0$ , an approximation as discussed in Section IV was used. In Section V we compare our results with the earlier correction factors and discuss means of improving the accuracy of the method.

### Equilibrium of a ring at liquid interface

When a circular ring of radii  $R$  and  $a$  is maintained horizontal at a fluid interface, the axisymmetric profiles of the inner and outer menisci formed around the ring may be described by their respective heights  $z_1(r)$  and  $z_2(r)$  from the flat level of the interface at distance  $r$  from the axis of symmetry (fig. 1). The equilibrium meniscus shapes are governed by the *Young-Laplace* equation of capillarity. When expressed in the dimensionless, parametric forms  $\bar{r}_i = \bar{r}_i(\phi_i)$  and  $\bar{z}_i = \bar{z}_i(\phi_i)$ , the equations describing meniscus shapes are (12)

$$\frac{\partial \bar{r}_i}{\partial \phi_i} = \frac{\bar{r}_i \cos \phi_i}{\bar{r}_i \bar{z}_i - \sin \phi_i}; \quad \frac{\partial \bar{z}_i}{\partial \phi_i} = \frac{\bar{r}_i \sin \phi_i}{\bar{r}_i \bar{z}_i - \sin \phi_i} \quad [2a, b]$$

where  $\phi_i$  is the angle between the axis of symmetry and the normal to the surface of the inner ( $i = 1$ ) meniscus or of the outer ( $i = 2$ ) meniscus. The definition of the slope angle  $\phi_2$  for the outer meniscus profile is chosen as shown in fig. 1, so that the above equations hold for both inner ( $i = 1$ ) and outer ( $i = 2$ ) menisci, and only the boundary conditions differ from each other (11, 12).

The solutions of eq. [2a, b] for the inner meniscus shapes are a family of curves of a single parameter introduced by *Bashforth* and *Adams* (11)

$$\beta_1 \equiv (\varrho_2 - \varrho_3) g b^2 / \gamma_{23} = (b\sqrt{C_{23}})^2$$

where  $b$  is the radius of curvature at the lowest point ( $r = 0$ ) of the meniscus. The shape

parameter is related to the height  $z_0$  of the point by (10)

$$\tilde{z}_0 = z_0/C_{23} = 2/\sqrt{\beta_1}.$$

An extensive and widely used tabulation of the solutions, the  $r$ - and  $z$ -coordinates of the curves as functions of  $\phi_1$  and  $\beta_1$ , is available (11)<sup>1)</sup>. The solutions of eq. [2a,b] for the outer meniscus shapes are again a family of curves of a single shape parameter. Hub and Scriven (12) chose  $\bar{r}_2$  at  $\phi_2 = 359.5^\circ$  as the shape parameter, which we may call  $\beta_2$  here; an extensive tabulation of these solutions is available (12).

The ring method requires that the inner and outer menisci meet the ring surface to make a zero angle of contact with it, so that we obtain at the lines of meniscus contact from the geometry (fig. 1)

$$\bar{R} = \bar{r}_{ic} + \bar{a} \sin \phi_{ic}, \quad [3]$$

$$\bar{b} = \bar{z}_{ic} - \bar{a} \cos \phi_{ic}, \quad i = 1, 2 \quad [4]$$

where  $\bar{r}_{ic}$  and  $\bar{z}_{ic}$  are the dimensionless coordinates of the contact line circle where the  $i$  meniscus meets the ring surface, and  $\phi_{ic}$  is the slope angle of the meniscus at the contact line. The coordinates should be the solutions of eq. [2a,b]. Eliminating  $\bar{b}$  from eq. [4], we get for  $\bar{R}$  and  $\bar{a}$ ,

$$\bar{R} = \frac{\bar{r}_{1c} \sin \phi_{2c} - \bar{r}_{2c} \sin \phi_{1c}}{\sin \phi_{2c} - \sin \phi_{1c}}, \quad [5]$$

$$\bar{a} = -\frac{\bar{r}_{2c} - \bar{r}_{1c}}{\sin \phi_{2c} - \sin \phi_{1c}} = \frac{\bar{z}_{2c} - \bar{z}_{1c}}{\cos \phi_{2c} - \cos \phi_{1c}}. \quad [6]$$

The second equality of eq. [6] yields

$$\frac{\bar{z}_{2c} - \bar{z}_{1c}}{\bar{r}_{2c} - \bar{r}_{1c}} = \tan \frac{1}{2}(\phi_{2c} + \phi_{1c}) \quad [7]$$

to provide the geometrical relation which two sets of values,  $(\phi_i; \bar{r}_i, \bar{z}_i)$ ,  $i = 1, 2$ , which are solutions of eq. [2a,b], must satisfy on the ring surface.

The dimensionless volume of the liquid raised above the  $\bar{z}=0$  plane can be calculated as (2)

$$\begin{aligned} \bar{v} = & 2\pi[(1 - \frac{1}{2}\bar{a}^2 \cos \phi_{ic})\bar{r}_{ic} \sin \phi_{ic} \\ & + (\bar{R} - \frac{1}{2}\bar{a} \sin \phi_{ic})\bar{a}\bar{z}_{ic} \sin \phi_{ic} \\ & + \frac{1}{2}\bar{a}^2 \bar{R} \phi_{ic} + \frac{1}{3}\bar{a}^3 \cos^3 \phi_{ic}]^{\frac{1}{2}} \end{aligned} \quad [8]$$

where

$$[ ]^{\frac{1}{2}} = [ ]_{i=1} - [ ]_{i=2}.$$

An equilibrium state of a ring of given  $\bar{R}$  and  $\bar{a}$  is determined, by locating two sets of values,  $(\phi_i; \bar{r}_i, \bar{z}_i)$ ,  $i = 1, 2$ , which are solutions of eq. [2a,b] and satisfy eqs. [5] and [6] at the contact line for a given  $\bar{b}$ . The dimensionless volume  $\bar{v}$  then follows from eq. [8]. For a ring of given  $\bar{R}$  and  $\bar{a}$ ,  $\bar{b}$  thus determines  $\bar{v}$  uniquely, and the parameters  $\beta_1$  and  $\beta_2$  are also determined to provide unique shapes of the menisci; alternatively, we may say that  $\bar{v}$  and  $\bar{b}$  are functions of  $\beta_1$  since, given the value of  $\beta_1$ ,  $\bar{v}$  and  $\bar{b}$  are fixed.

The maximum  $\bar{v}$  is calculated by considering  $\bar{b}$  to vary continuously, with accompanying variations of  $\beta_1$  and  $\bar{v}$ . When  $\bar{v}$  attains a maximum, we have (fig. 2)

$$\frac{d\bar{v}}{d\bar{b}} = \frac{d\bar{v}/d\beta_1}{d\bar{b}/d\beta_1} = 0, \text{ or } \frac{d\bar{v}}{d\beta_1} = 0 \text{ if } \frac{d\bar{b}}{d\beta_1} \neq 0$$

where  $\bar{v}$  of eq. [8] is the function of the variables,  $\phi_{ic}(\beta_i)$ ,  $\bar{r}_{ic}[\phi_{ic}(\beta_i), \beta_i]$  and  $\bar{z}_{ic}[\phi_{ic}(\beta_i), \beta_i]$ ,  $i = 1, 2$ , and  $\beta_2$  is in turn a function of  $\beta_1$ . Differentiating  $\bar{v}$  with respect to  $\beta_1$ , we get

$$\begin{aligned} \frac{d\bar{v}}{d\beta_1} = 0 = & 2\pi \left[ \left\{ (1 - \frac{1}{2}\bar{a}^2 \cos \phi_{ic}) \sin \phi_{ic} \frac{\partial \bar{r}_{ic}}{\partial \phi_i} \right. \right. \\ & + (\bar{R} - \frac{1}{2}\bar{a} \sin \phi_{ic})\bar{a} \sin \phi_{ic} \frac{\partial \bar{z}_{ic}}{\partial \phi_i} \\ & + (1 + \bar{a}\bar{z}_{ic})\bar{r}_{ic} \cos \phi_{ic} + (\bar{r}_{ic} \sin \phi_{ic} \\ & \left. \left. - \frac{1}{2}\bar{a} \cos 2\phi_{ic}\right) \bar{a}^2 \sin \phi_{ic} \right\} \frac{d\phi_{ic}}{d\beta_i} \frac{d\beta_i}{d\beta_1} \\ & + (1 - \frac{1}{2}\bar{a}^2 \cos \phi_{ic}) \sin \phi_{ic} \frac{\partial \bar{r}_{ic}}{\partial \beta_i} \frac{d\beta_i}{d\beta_1} \\ & + (\bar{R} - \frac{1}{2}\bar{a} \sin \phi_{ic})\bar{a} \sin \phi_{ic} \frac{\partial \bar{z}_{ic}}{\partial \beta_i} \frac{d\beta_i}{d\beta_1} \Big]^{\frac{1}{2}} \end{aligned} \quad [9]$$

where  $\partial \bar{r}_{ic}/\partial \phi_i$  and  $\partial \bar{z}_{ic}/\partial \phi_i$  may be expressed in terms of  $(\phi_{ic}; \bar{r}_{ic}, \bar{z}_{ic})$  by eq. [2a,b].

At the lines of contact, conditions [3] and [4] must apply whatever the value of  $\beta_1$ , so

<sup>1)</sup> See also J. F. Padday, in: E. Matijevic (Ed.), Surface and Colloid Science, Vol. 1, 151 (New York 1969).

that they may be differentiated with respect to  $\beta_1$  to yield

$$0 = \left( \frac{\partial \bar{r}_{ic}}{\partial \phi_i} + \bar{a} \cos \phi_{ic} \right) \frac{d\phi_{ic}}{d\beta_i} \frac{d\beta_i}{d\beta_1} + \frac{\partial \bar{r}_{ic}}{\partial \beta_i} \frac{d\beta_i}{d\beta_1}, \quad i=1,2, \quad [10]$$

$$\left[ \left( \frac{\partial \bar{x}_{ic}}{\partial \phi_i} + \bar{a} \sin \phi_{ic} \right) \frac{d\phi_{ic}}{d\beta_i} \frac{d\beta_i}{d\beta_1} + \frac{\partial \bar{x}_{ic}}{\partial \beta_i} \frac{d\beta_i}{d\beta_1} \right]_2 = 0 \quad [11]$$

It is convenient (5) to express the variations of  $\bar{r}_{ic}$  and  $\bar{x}_{ic}$  in  $\beta_i$  in terms of a newly-defined quantity:

$$\lambda_i(\phi_i, \beta_i) = \frac{1 + \tan \phi_i \left( \frac{\partial \bar{x}_i}{\partial \beta_i} / \frac{\partial \bar{r}_i}{\partial \beta_i} \right)}{\tan \phi_i - \left( \frac{\partial \bar{x}_i}{\partial \beta_i} / \frac{\partial \bar{r}_i}{\partial \beta_i} \right)}. \quad [12]$$

From eqs. [9] to [12], we can eliminate  $\partial \bar{r}_{ic} / \partial \beta_i$ ,  $\partial \bar{x}_{ic} / \partial \beta_i$ ,  $d\phi_{ic} / d\beta_i$ ,  $i=1,2$ , and the condition of the maximum  $\bar{v}$  can be expressed in terms of  $\lambda_{ic}$ :

$$[\mathcal{A}_{ic}]_2^1 = 0 \quad [13]$$

where

$$\mathcal{A}_i \equiv (\cos \phi_i \lambda_i + \sin \phi_i) \cos \phi_i (\bar{r}_i \bar{x}_i - \sin \phi_i) - \frac{\bar{r}_i^2}{2}, \quad [13a]$$

and the subscript  $c$  denotes values at the contact line. This is the condition at the state of the maximum volume  $\bar{v} = \bar{V}$ . As  $\bar{r}_i$  and  $\bar{x}_i$  are known as functions of  $\beta_i$  and  $\phi_i$  (11, 12),  $\lambda_i$  may be calculated; however, it proves to be more efficient (5) to differentiate eq. [2a,b] with respect to  $\beta_i$ , and to obtain a differential equation for  $\lambda_i$  in terms of  $\phi_i$  by eliminating the resulting  $\partial \bar{r} / \partial \beta_i$  and  $\partial \bar{x} / \partial \beta_i$ :

$$(\bar{r}_i \bar{x}_i - \sin \phi_i)^2 \left( \frac{\partial \lambda_i}{\partial \phi_i} + \lambda_i^2 \right) + \sin \phi_i (\bar{r}_i^2 + \cos \phi_i) \lambda_i + (\bar{r}_i^2 \bar{x}_i^2 - 2 \bar{r}_i \bar{x}_i \sin \phi_i + 2 \sin^2 \phi_i - \bar{r}_i^2 \cos \phi_i) = 0 \quad [14]$$

in which  $\bar{r}_i$  and  $\bar{x}_i$  are the solutions of eq. [2a,b]. Integrating eq. [14] with respect to

$\phi_i$ , we can obtain  $\lambda_i$  for the desired values of  $(\phi_i, \beta_i)$ . The methods of integrating eq. [14] for  $\lambda_i$  are discussed elsewhere (5, 13), and will be used without further elaboration in the next section where the detailed method of numerical calculation of the maximum volume  $\bar{V}$  is discussed.

As pointed out earlier, the equilibrium of the ring at the interface may be maintained beyond the position of maximum force (fig. 2). It is of interest to know the maximum equilibrium height of the ring at the interface, and to see how much it exceeds that for the maximum force. At the maximum height, the following should hold (5):

$$\frac{db}{d\bar{v}} = \frac{db/d\beta_1}{d\bar{v}/d\beta_1} = 0, \text{ or } \frac{db}{d\beta_1} = 0 \text{ if } \frac{d\bar{v}}{d\beta_1} \neq 0. \quad [15]$$

Combining eqs. [10] and [11] with eq. [15], we get as the condition for the maximum  $\bar{b}$

$$\begin{aligned} & \left( \frac{\bar{r}_{ic}}{\bar{r}_{ic} \bar{x}_{ic} - \sin \phi_{ic}} + \bar{a} \right) \\ & \times \left( \cos \phi_{ic} \frac{\partial \bar{x}_{ic}}{\partial \beta_i} - \sin \phi_{ic} \frac{\partial \bar{r}_{ic}}{\partial \beta_i} \right) = 0, \quad i=1,2. \end{aligned} \quad [16]$$

Since the terms in the first bracket do not vanish in general, those in the second do, which is equivalent to the condition

$$\lambda_{ic} \rightarrow \infty, \quad i=1,2. \quad [17]$$

We see that eq. [17] is the condition for the limit of stability for the equilibrium meniscus formed around a solid whose position in space is fixed (13). Condition [17] may be satisfied either by the inner ( $i=1$ ) or by the outer meniscus ( $i=2$ ), and when one becomes unstable, it should lead to the detachment of the ring even though the other meniscus is stable. From the solutions of eq. [14], we can examine whether or not a particular state of the ring at the interface satisfies eq. [17], and thus reaches the maximum height in accordance with eq. [15]. Unlike the case of the sphere (5, 7), however, a further consideration is necessary: the possibility that the two menisci approach one another so closely that the thin film intervening them ruptures, before the menisci instability occurs (8, 14). When

the equilibrium state of eq. [15] is established, we should therefore examine whether or not the inner and outer meniscus curves either intersect or touch one another: if so, the height obtained by eq. [15] is meaningless, because the thin film intervening the two menisci can rupture before this height is attained.

## Numerical calculations and results

To calculate the maximum  $\bar{v}$  for a ring of given  $\bar{R}$  and  $\bar{a}$ , we must find two sets of values,  $(\phi_i; \bar{r}_i, \bar{\chi}_i; \lambda_i)$ ,  $i = 1, 2$ , which are solutions of eqs. [2a,b] and [14] and satisfy eqs. [5], [6] and [13] at the contact lines;  $\bar{v}$  is calculated from eq. [8]. These being difficult tasks to perform, we adopt a scheme in which we attempt to find the two sets,  $(\phi_i; \bar{r}_i, \bar{\chi}_i; \lambda_i)$ ,  $i = 1, 2$ , which are solutions of eqs. [2a,b] and [14], and satisfy only the geometrical condition [7] and the maximum-volume condition [13]. In so doing we define a state of the maximum  $\bar{v}$  for the yet-unknown values of  $\bar{R}$  and  $\bar{a}$ , which we calculate from eqs. [5] and [6]. We do this for a sufficiently large number of the sets,  $(\phi_i; \bar{r}_i, \bar{\chi}_i; \lambda_i)$  to warrant the interpolation of the maximum volume  $\bar{V}$  for the desired  $\bar{R}$  and  $\bar{a}$ .

To satisfy the maximum-volume condition [13], we observe that  $A_i$  of eq. [13a] depends only on  $(\phi_i; \bar{r}_i, \bar{\chi}_i; \lambda_i)$  of one meniscus and not on the dimensions of the ring and the other meniscus. When we numerically integrate the differential equations [2a,b] and [14] for  $(\phi_i; \bar{r}_i, \bar{\chi}_i; \lambda_i)$ , therefore, we can store in the computer the values of  $(\phi_i; \bar{r}_i, \bar{\chi}_i)$  at the uniform interval of  $A_i$ . The method of integration and its accuracy are discussed elsewhere (5); the method is adopted here without modification.

For a fixed  $A_i = A_0$ , a multitude of the sets  $(\phi_i; \bar{r}_i, \bar{\chi}_i)_{A_i=A_0}$  are thus generated for various values of  $\beta_i$ . Any pair of sets  $(\phi_1; \bar{r}_1, \bar{\chi}_1)_{A_1=A_0}$  and  $(\phi_2; \bar{r}_2, \bar{\chi}_2)_{A_2=A_0}$  of the same  $A_0$  will then satisfy eq. [13]. For the set  $(\phi_1; \bar{r}_1, \bar{\chi}_1)_{A_1=A_0}$  of a particular  $\beta_1$ , we can find the corresponding set, which together with it satisfies eq. [7], among the multitude of the sets  $(\phi_2; \bar{r}_2, \bar{\chi}_2)$  of the same  $A_0$ . In actuality, this requires the interpolations of the values  $(\phi_2)$ ,  $(\bar{r}_2)$  and  $(\bar{\chi}_2)$  for different  $\beta_2$ 's; a standard IBM subroutine for the Aitken-Lagrange interpolation is employed, taking 6 closest data points and with the upper error bounds of  $10^{-7}$ . The pair of sets  $(\phi_i; \bar{r}_i, \bar{\chi}_i)_{A_i=A_0}$ ,  $i = 1, 2$ , thus obtained define a state of the maximum  $\bar{V}$ . The corresponding  $\bar{R}$ ,  $\bar{a}$  and  $\bar{V}$  can

Table 1. Generation of the data points for  $A_0 = -0.1$

$\beta_2$	$\phi_2$	$\bar{r}_2$	$\bar{\chi}_2$	Data Point No.	$\beta_1$	$\phi_1$	$\bar{r}_1$	$\bar{\chi}_1$
4.865	102.1542	1.104652	1.128586	1	5.15	34.23825	1.095008	1.191616
4.880	102.3395	1.115449	1.133098	2	5.27	33.87368	1.096913	1.178551
4.985	102.5251	1.126291	1.137589	3	5.35	33.63698	1.098139	1.170075
4.910	102.7109	1.137180	1.142059	4	5.41	33.46265	1.099036	1.163837
4.925	102.8970	1.148115	1.146510	5	5.46	33.31943	1.099769	1.158715
4.940	103.0832	1.159093	1.150939	6	5.50	33.20615	1.100346	1.154665
4.955	103.2696	1.170117	1.155349	7	5.54	33.09402	1.100916	1.150658
4.970	103.4562	1.181185	1.159738	8	5.57	33.01068	1.101339	1.147680

Data Point No.	$\phi_2$	$\bar{r}_2$	$\bar{\chi}_2$	$R/a$	$R^3/V$	$f$
1	103.0339	1.156185	1.149769	28.07126	0.1220391	1.228253
2	102.8494	1.145317	1.145373	35.28240	0.1231746	1.246109
3	102.7280	1.138178	1.142468	42.49902	0.1239452	1.258142
4	102.6453	1.133335	1.140479	49.48456	0.1245161	1.266715
5	102.5770	1.129338	1.138832	57.28068	0.1249953	1.273888
6	102.5048	1.125093	1.137104	68.30782	0.1254175	1.280906
7	102.4740	1.123316	1.136342	75.36951	0.1257585	1.285060
8	102.4508	1.121973	1.135768	81.74408	0.1260150	1.288196

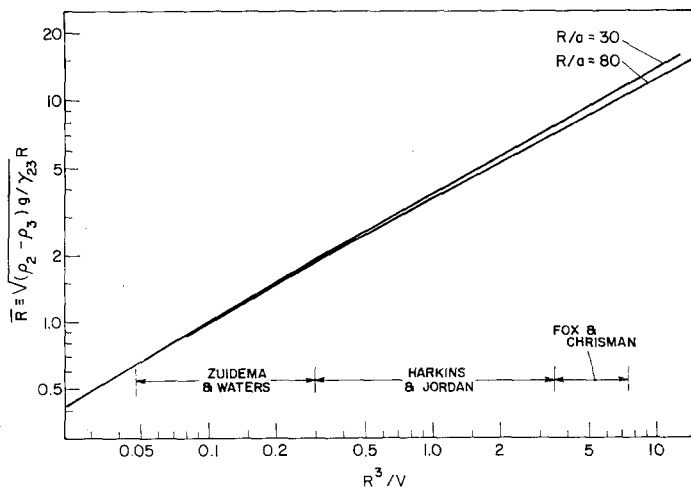


Fig. 3.  $\bar{R}$  as a function of  $R^3/V$  and  $R/a$ . The applicable ranges of the factor  $f$  which are obtained experimentally and available in the literature, are shown

be calculated from eqs. [5], [6], and [8], respectively.

The results of the operation performed by the computer for the particular value of  $A_0 = -0.1$  are listed in table 1 to illustrate this process. For 50 values of  $A_0$  ranging from  $-0.002$  to  $-40.0$ , operations similar to that of Table 1 have been performed, each generating 8 data points. From the total of 400 data points accordingly produced, a table of the factor  $f$  as a function of  $R^3/V$  and  $R/a$  has been constructed using the interpolation subroutine. The range of  $R^3/V$  and  $R/a$  of the 97-page tabulation, which is not included here\*), is

$$R/a = 30(1)80, \text{ and}$$

$$R^3/V = 0.025(0.001)0.040(0.002)0.100(0.005) \\ 0.30(0.01)0.60(0.02)2.00(0.05)5.00,$$

where the intervening quantities in parentheses indicate the intervals of values tabulated. An additional tabulation of  $f$  was constructed, using the approximate solutions discussed in the next Section, for the range of the same  $R/a$  and

$$R^3/V = 5.1(0.1)20.0^*.$$

In fig. 3, the parameter ranges of our calculations are compared to the ranges available in the literature. Fig. 4(a) shows  $f$  in the range of  $R^3/V = 0.025$  to  $0.4$ ; 4(b) in the range  $0.4$  to  $4.6$ ; and 4(c)  $1.3$  to  $10$ .

Since we know  $(\beta_i, \phi_i, \bar{r}_i, \bar{\chi}_i)$ ,  $i = 1, 2$ , for a given set of  $(\bar{R}, \bar{a}, \bar{V})$ , we can calculate, in addition to  $f$ , various supplementary data on the state of the ring at the liquid interface, which can be used to increase the accuracy of the ring method. Fig. 3 shows  $\bar{R}$  as a function of  $R^3/V$  and  $R/a$ , and may be used to find the approximate value of  $R^3/V$  before starting a measurement if  $\gamma_{23}$  is roughly known. Fig. 5(a) shows the shape parameter  $\beta_1$  of the inner meniscus and its dimensionless height  $\bar{\chi}_0$  at  $\bar{r} = 0$  as functions of  $R^3/V$  and  $R/a$ . Fig. 5(b) shows the shape parameter  $\beta_2(\bar{r}_2$  at  $\phi_2 = 359.5^\circ)$  of the outer meniscus as a function of  $R^3/V$  and  $R/a$ . These two figures identify the shapes of the inner and outer menisci attached to the ring of given  $R$  and  $a$  in the critical state. Fig. 6(a) shows the location of the contact line circle where the inner meniscus meets the ring surface at the critical state, as a function of  $R^3/V$  and  $R/a$ . The location is expressed in terms of  $\psi_1$ , the angle between the lines drawn from the center of the ring wire, vertically downwards and to the contact line (fig. 1). Fig. 6(b) shows the location  $\psi_2$  of the contact line circle where the outer meniscus meets the ring surface in the critical state. As described in Section V, figs. 6(a) and (b) are of use in judging if the attachment of the support wire to the ring wire interferes with the contact lines on the surface of the

\*) See NAPS document deposit for 97 pages of tabulation. Order from ASIS/NAPS c/o Microfiche Publications, 305 E. 46th St., New York, N.Y. 10017, citing the reference of this paper. Remit in advance \$ 1.50 for a microfiche or \$ 15.05 for a photocopy. This includes a tabulation of  $\bar{v}$  for the menisci in contact as a function of  $\bar{R}$  and  $R/a$ , as discussed later.

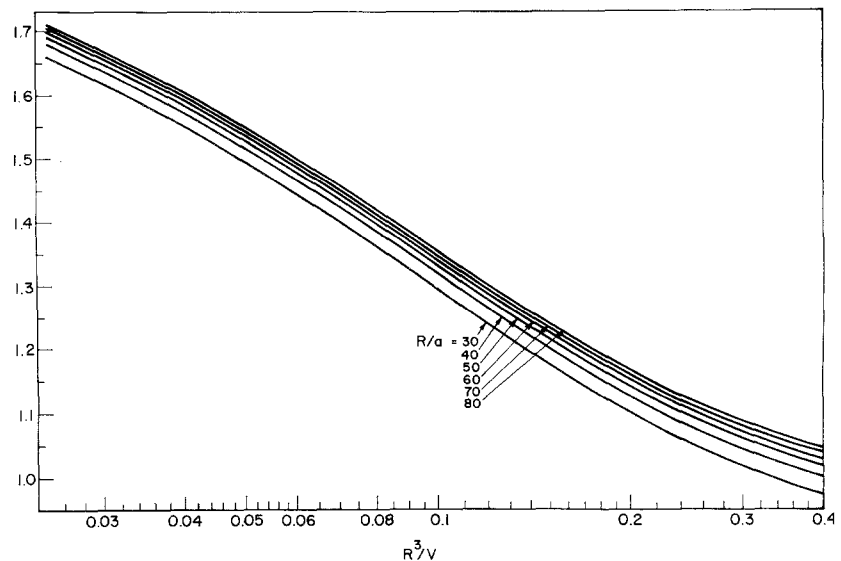


Fig. 4(a). The factor  $f$  in the range of  $R^3/V = 0.025$  to  $0.4$  and  $R/a = 30$   $80$  to

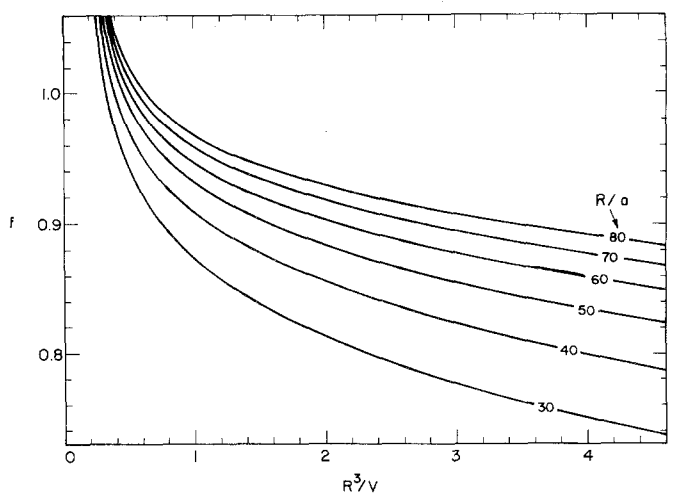


Fig. 4(b). The factor  $f$  in the range of  $R^3/V = 0.4$  to  $4.5$  and  $R/a = 30$   $80$  to

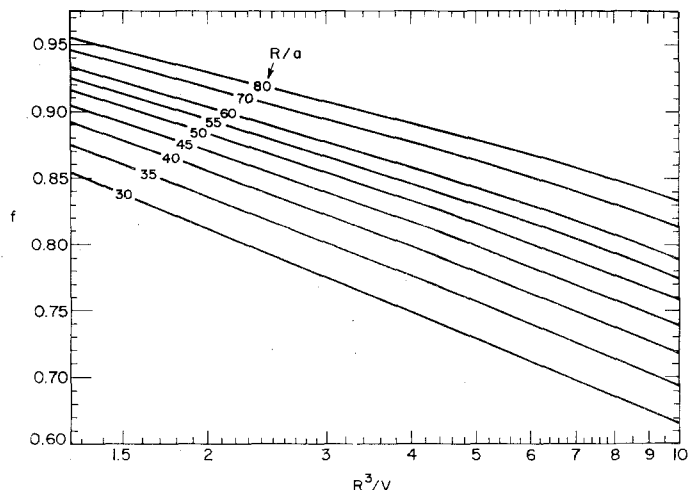


Fig. 4(c). The factor  $f$  in the range of  $R^3/V = 1.3$  to  $10.0$  and  $R/a = 30$  to  $80$

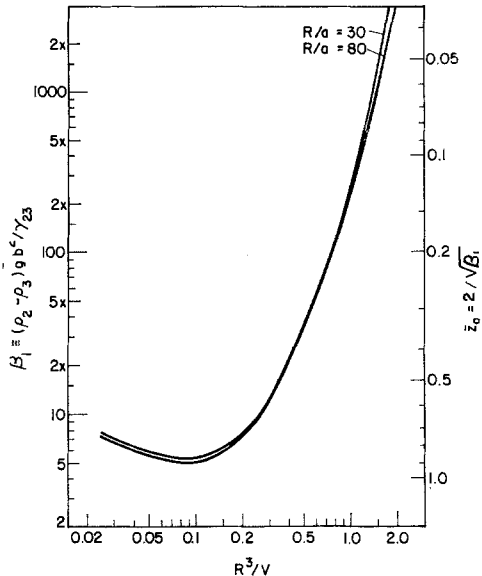


Fig. 5(a). The shape parameter  $\beta_1$  of the inner meniscus and its dimensionless height  $\bar{z}_0$  at  $\bar{r}=0$  above the flat level of the interface, as functions of  $R^3/V$  and  $R/a$

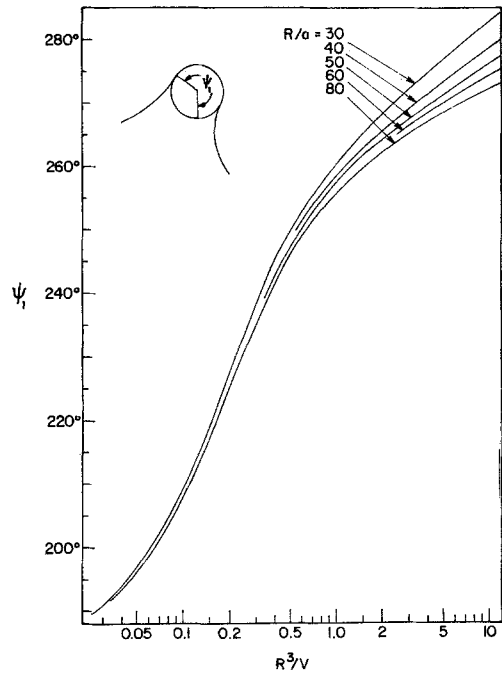


Fig. 6(a). The location  $\psi_1$  of the contact line circle where the inner meniscus meets the ring surface at the critical state, as a function of  $R^3/V$  and  $R/a$

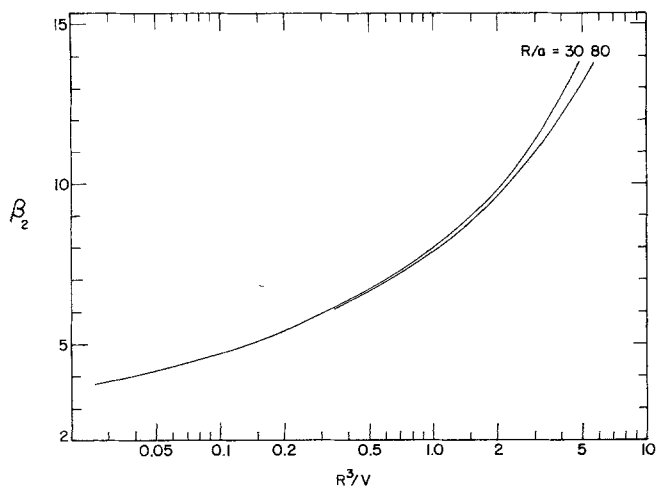


Fig. 5(b). The shape parameter  $\beta_2$  ( $\bar{r}_2$  at  $\phi_2 = 359.5^\circ$ ) of the outer meniscus as a function of  $R^3/V$  and  $R/a$

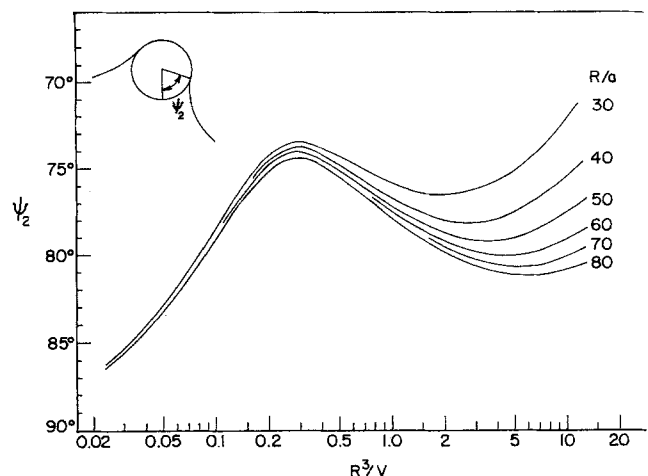


Fig. 6(b). The location  $\psi_2$  of the contact line circle where the outer meniscus meets the ring surface at the critical state, as a function of  $R^3/V$  and  $R/a$

ring wire maintaining axial symmetry in the critical state.

Just as eq. [13] determines the maximum  $\bar{v}$  for a ring of given  $\bar{R}$  and  $\bar{a}$ , eq. [17] determines the maximum  $\bar{h}$  for given  $\bar{R}$  and  $\bar{a}$ , provided the thin film between the inner and outer menisci does not rupture at a smaller  $\bar{h}$ . To calculate the maximum  $\bar{h}$ , we

find a set  $(\phi_i; \bar{r}_i, \bar{z}_i; \lambda_i = \infty)$  from the solutions of eqs. [2a,b] and [14], and attempt to find  $(\phi_j; \bar{r}_j, \bar{z}_j)$  for the other meniscus ( $j \neq i$ ) which together with the above set, satisfy eq. [17]. In so doing we define a state of the maximum  $\bar{h}$  according to eq. [15] for the yet-unknown values of  $\bar{R}$  and  $\bar{a}$ , which we calculate from eqs. [5] and [6]. Having calculated  $\bar{h}$  according

to eq. [15], we must establish whether or not the inner and outer meniscus curves for the height either intersect or touch one another. From such calculations in the range of  $\bar{R} = 1.9$  to 5.2 and  $R/a = 30$  to 80, we have found that the inner and outer meniscus curves always intersect one another. The ring will therefore detach from the interface by rupture of the intervening film before this height is attained. This will occur when surface active agents are absent; when they are present so that the interfacial tensions are variable (i.e. the film is elastic) one cannot predict when rupture will occur (14). We have also found that for the entire range of our calculations, the two meniscus curves neither intersect nor touch one another at the maximum  $\bar{V}$ .

The ring height at the rupture can be calculated theoretically, if we assume that the rupture occurs at the instant when the inner and outer menisci come into contact with each other. The ring height when the menisci make contact is calculated, first by locating for a given inner meniscus the outer meniscus which just touches it, without regard to the presence of the ring, and then by "fitting" the rings between the two menisci above the point of contact (fig. 7). For 12 profiles of the inner meniscus ( $\beta_1 = 10^1 - 8 \times 10^6$ ), the corresponding profiles of the outer meniscus which comes into contact are calculated numerically. The profile curves are obtained, as before (5), by integrating eqs. [2a, b] using the *Runge-Kutta* method, which is available as a standard subroutine programmed in the IBM S360 computer. The integration increment of

$\Delta\phi_i = 0.5^\circ$  and the upper error bounds of  $10^{-9}$  are again adopted. The value of  $\beta_2$  for a given  $\beta_1$  is listed in table 2, each pair of menisci being separated at the distance  $\Delta \leq 0.002$ . The outer meniscus profiles whose value of  $\beta_2$  deviates  $\pm 0.001$  from the listed  $\beta_2$ , resulted in greater separation of the inner and outer menisci. Table 2 also provides the coordinates of the point on the outer meniscus which is closest to the inner meniscus, which may be considered to be the approximate location of the contact point with the accuracy of  $\Delta$ . It will be noted that the height of the contact points is approximately constant at  $\sqrt{2}$ , suggesting that there may be a simple physical explanation; however, we have been unable to find any.

Table 2. The inner and outer menisci in contact and the approximate location of the contact point

$\beta_1$	$\beta_2$	$\phi_2$ (deg.)	$\bar{r}_2$	$\bar{z}_2$	$\Delta$
10	5.685	239.0	1.7887	1.4161	0.0010
20	6.224	245.6	2.2090	1.4182	0.0014
50	6.851	250.9	2.7368	1.4169	0.0006
100	7.299	253.5	3.1310	1.4159	0.0012
200	7.738	255.5	3.5267	1.4152	0.0017
500	8.289	257.4	4.0334	1.4150	0.0020
1000	8.699	258.6	4.4156	1.4146	0.0006
5000	9.631	260.5	5.2970	1.4145	0.0004
$10^4$	10.026	261.2	5.6744	1.4144	0.0004
$10^5$	11.312	262.8	6.9144	1.4143	0.0007
$10^6$	12.571	263.9	8.1400	1.4143	0.0002
$8 \times 10^6$	13.693	264.6	9.2386	1.4140	0.0006

$\Delta \equiv$  Minimum distance between the menisci of the listed  $\beta_1$  and  $\beta_2$ .

The coordinates designate the point on the outer meniscus which is closest to the inner meniscus.

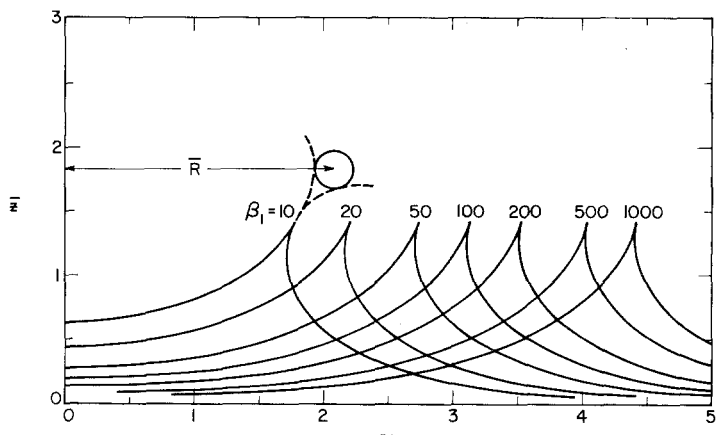


Fig. 7. The inner and outer menisci in contact, and the "fitting" of the rings between the menisci above the contact point

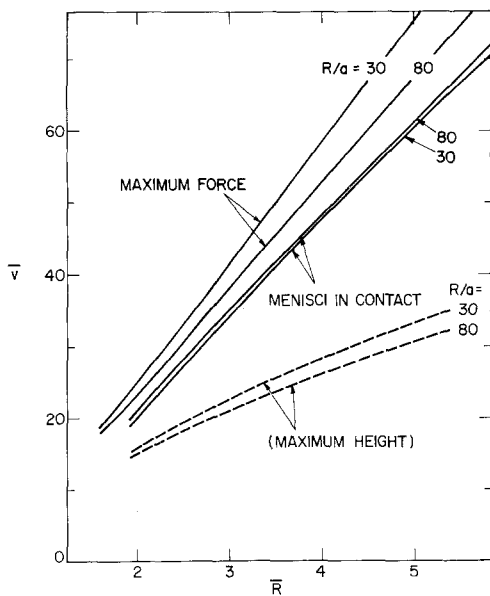


Fig. 8. Comparison of  $\bar{v}$  for the maximum  $\bar{V}$ , for the ring height according to eq. [15], and for menisci in contact

$$R/a = 30(1)80 \text{ and} \\ \bar{R} = 2.1(0.1)5.0(0.2)9.0,$$

where the intervening quantitites in parentheses again indicate the intervals of values tabulated. This tabulation has been deposited with the tabulation of  $f$ .

### Approximate solutions for large $R^3/V$

When  $R^3/V > 5.0$ , the ring radius is so large compared to the dimensions of the inner and outer menisci that their shape deviates only slightly from that of the cylindrical meniscus [e.g., eqs. (29) and (30) of Ref. (10)], whose principal curvature in the azimuthal direction vanishes. At  $A_0 = -40$ ,  $\beta_1$  ranges from  $3.41 \times 10^6$  for  $R/a = 30$  ( $R^3/V = 4.816$ ) to  $4.78 \times 10^6$  for  $R/a = 80$  ( $R^3/V = 5.714$ ). However, the effect of the azimuthal curvature is not negligible: the surface profiles of the inner and outer menisci, though almost of the cylindrical meniscus, are not symmetric with respect to the vertical line drawn through the center of the ring wire, as we can observe by comparing figs. 6(a) and 6(b). Thus, for  $R^3/V = 4.816$  and  $R/a = 30$ , the inner contact line circle locates at  $\psi_1 \approx 276.2^\circ$  while the outer contact line circle stays at  $\psi_2 \approx 75.4^\circ$ . Were the menisci truly cylindrical, this would have been at  $\psi_2 \approx 360^\circ - 276.2^\circ \approx 83.8^\circ$ .

To treat such systems, we employ the approximate solutions for the equilibrium shapes of axisymmetric menisci whose azimuthal curvature is much smaller than the meridional curvature. The approximate solution derived by Rayleigh (15) for the shape of large sessile drops builds on the solution for the cylindrical surface the correction arising from the contribution of the small azimuthal curvature:

$$\frac{\tilde{x}_i^2}{4} - \sin^2\left(\frac{\phi_i}{2}\right) + (-1)^i \frac{2}{3\bar{r}_i} \times \left[1 - \cos^3\left(\frac{\phi_i}{2}\right)\right] = 0, \quad i = 1, 2, \quad [18]$$

which we may use for the inner meniscus shape ( $i = 1$ ). With the change of the sign indicated ( $i = 2$ ), the equation should also hold for the outer meniscus. The value of  $\lambda_i$  can be obtained by differentiating the above equation with respect to  $\beta_i$ , and inserting eq.

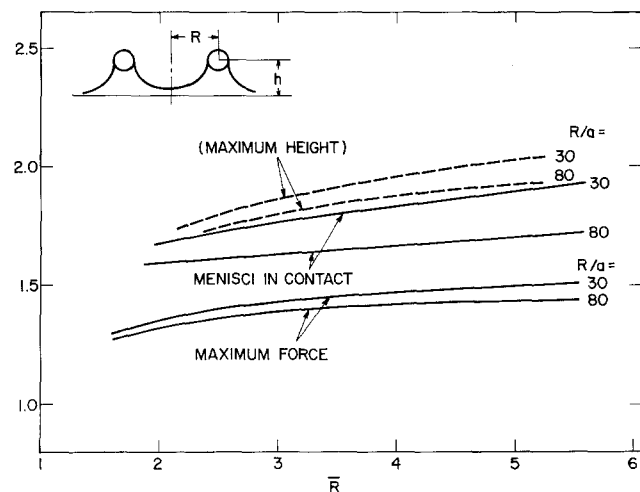


Fig. 9. Comparison of  $\bar{b}$  for the maximum  $\bar{V}$ , for the ring height according to eq. [15], and for menisci in contact

After the profiles in contact are calculated, the rings are “fitted” in between the two menisci to provide  $\bar{v}$  and  $\bar{b}$  as functions of  $\bar{R}$  and  $R/a$ . Fig. 8 compares  $\bar{v}$  for the maximum  $\bar{V}$ , for the ring height according to eq. [15], and for the menisci in contact. Fig. 9 compares  $\bar{b}$  for the three states. As a matter of interest, we have constructed a tabulation of  $\bar{v}$  for the menisci in contact as a function of  $\bar{R}$  and  $R/a$ , in the ranges of

[12] for  $\lambda_i$ :

$$\lambda_i = \frac{\bar{r}_i^2 \tilde{\chi}_i \cos \phi_i + (-1)^i \frac{4}{3} \left[ 1 - \cos^3 \left( \frac{\phi_i}{2} \right) \right] \sin \phi_i}{\bar{r}_i^2 \tilde{\chi}_i \sin \phi_i - (-1)^i \frac{4}{3} \left[ 1 - \cos^3 \left( \frac{\phi_i}{2} \right) \right] \cos \phi_i},$$

$$i = 1, 2.$$
[19]

The method of obtaining the maximum  $\bar{v}$  is the same as before, except that eqs. [18] and [19] are used instead of eqs. [2a, b] and [14] numerically integrated, to calculate  $(\phi_i; \bar{r}_i, \tilde{\chi}_i, \lambda_i)$ .

The results of the calculations, which list  $f$  as a function of  $R^3/V = 5.1$  to 20.0 at the interval of 0.1, and  $R/a = 30$  to 80 at the interval of 1, are included in the deposited tables. Table 3 compares the approximate solution with the exact values in the range of  $R^3/V = 4.5$  to 5.0. We note that in view of the simplicity of eq. [18], the numerical computations are considerably shortened. The agreement becomes poorer as the radius ratio  $R/a$  becomes smaller, because of the increasing effect of the azimuthal curvature of the ring.

## Discussion

We compare in table 4 (a) our results with the values of the factor  $f$  obtained experimentally by *Harkins and Jordan* (1). The results are in good agreement, the largest deviation being about 1.1%, but generally less than 0.4%, and their results are consistently lower than ours. We believe that their values are indeed lower than the true values, because *Fox and Chrisman* (3) with their experiments made the same observation as we did. Table 5 compares the surface tension values they obtained by the capillary-rise method and by the ring method. The values of  $f$  of *Harkins and Jordan* are shown to provide the surface tension values always lower than those from the capillary-rise method; when our results are used, the values by the two methods prove to agree very well. The values of  $f$  obtained by *Fox and Chrisman* for  $R^3/V > 3.5$  are compared with our results in table 4 (b). They show good agreement for  $R/a = 54$ , for which they performed their experiments, but the extrapolation of the results to the radius ratio other than 54 is poor. Table 4 (c) compares for  $R^3/V < 0.30$  the values of  $f$  obtained by *Zuidema and Waters* (4)

Table 3. Comparison of the approximate and exact values of  $f$

$R/a$	$R^3/V$	Approximate	Exact	% Deviation
30	4.5	0.7396	0.7387	+0.12%
	4.7	0.7355	0.7346	+0.12%
	5.0	0.7297	0.7292	+0.07%
	4.5	0.8510	0.8505	+0.06%
	4.7	0.8478	0.8476	+0.02%
	5.0	0.8434	0.8431	+0.04%
60	4.5	0.8850	0.8850	0.00%
	4.7	0.8829	0.8823	+0.07%
	5.0	0.8792	0.8787	+0.06%

Table 4. Comparison with previous values of  $f$

(a) Comparison with <i>Harkins and Jordan</i> (1)				
$R/a$	$R^3/V$	<i>H. J.</i>	Present	% Difference
30	0.3	1.012	1.0155	-0.34%
	1.0	0.8734	0.8737	-0.03%
	3.5	0.7542	0.7621	-1.04%
	4.0	1.038	1.0425	-0.43%
	1.0	0.9047	0.9091	-0.48%
	3.5	0.8057	0.8107	-0.62%
40	0.4	1.022	1.0289	-0.67%
	1.0	0.9438	0.9472	-0.36%
	3.5	0.8668	0.8676	-0.09%
	80	1.6	0.9365	-0.51%
	3.5	0.8974	0.8993	-0.21%
(b) Comparison with <i>Fox and Chrisman</i> (3)				
		<i>F. C.</i>	Present	
40	3.5	0.8063	0.8107	-0.54%
	5.5	0.7645	0.7723*)	-1.01%
	7.5	0.7302	0.7442*)	-1.88%
	54	0.852	0.8542	-0.26%
	4.5	0.835	0.8358	-0.10%
	5.5	0.821	0.8210*)	0.00%
60	7.5	0.797	0.7959*)	+0.14%
	3.5	0.8672	0.8676	-0.05%
	5.5	0.8389	0.8363*)	+0.31%
	7.5	0.8168	0.8125*)	+0.53%
(c) Comparison with <i>Zuidema and Waters</i> (4)				
		<i>Z. W.</i>	Present	
30	0.05	1.4756	1.4965	-1.40%
	0.10	1.2507	1.2946	-3.39%
	0.30	1.0166	1.0155	+0.18%
	40	0.05	1.4849	-2.15%
	0.10	1.2639	1.3181	-4.12%
	0.30	1.0397	1.0425	-0.27%
60	0.05	1.4940	1.5401	-2.99%
	0.10	1.2767	1.3422	-4.88%
	0.30	1.0612	1.0705	-0.87%

\*) Approximate solution which differs from the exact value at most +0.15%.

with ours. Near  $R^3/V = 0.30$ , the lower limit of the *Harkins-Jordan* tabulation, their results agree well with ours. If  $R^3/V$  deviates

Table 5. Experimental data of Fox and Chrisman (3)

Compound	$R^3/V$	capillary-ring*†) rise*)	% Difference
Water	0.92	72.75 (a) 72.57	-0.25 % 0.00 %
		(b) 72.75	0.00 %
Benzene	1.93	28.86 (a) 28.76	-0.35 % 0.00 %
		(b) 28.86	0.00 %
Hexadecane	1.80	27.60 (a) 27.44	-0.58 % -0.22 %
		(b) 27.54	0.00 %
Hexadeca-			
methylhept-			
asiloxane	3.14	18.61 (a) 18.53	-0.43 % -0.11 %
		(b) 18.59	0.00 %

\*) Surface tension in dynes/cm at 20 °C.

†) (a) using the correction factors of Harkins and Jordan (1); (b) using those of this paper. The radius ratio of the ring used is  $R/a = 54$ .

much from 0.30, their results however are very poor, the deviation from our results being as high as 5%.

When the interfacial tension of an immiscible liquid/liquid system is measured, and the upper liquid completely wets the ring surface rather than the lower one, the downward force necessary to detach the ring from the interface must be measured rather than the upward force, but otherwise the procedure is identical. This is because the system has a bilateral symmetry with respect to the horizontal plane,  $z = 0$  (5). Some commercial rings cannot be displaced downwards to overcome the maximum force of detachment by their own weight, and require an elaborate accessory for the purpose. If a ring made of a thick wire is chosen (or a dead weight is attached to the ring with some commercial rings), such an accessory may not be needed. When a rough estimate of  $\gamma_{23}$  is available for a system, fig. 3 can be used to determine for a given  $R$  the maximum equilibrium force of detachment which should be overcome. From the  $R$  calculated using approximate  $\gamma_{23}$ ,  $R^3/V$  is read and  $V$  is subsequently calculated; the maximum force to be overcome is  $(\rho_2 - \rho_3)gV$ . It should be remembered that the point of zero force should be established in the phase into which the ring is pulled.

The difficulty in using the ring method to measure the interfacial tension of immiscible liquid/liquid systems is illustrated by the experimental data presented by Harkins and Jordan (1). As shown in table 6, several values

of  $f$  obtained by them via interfacial-tension measurements deviate more from our results than those via surface-tension measurements. As Harkins and Jordan noted, it is difficult to assure that one of the liquids completely wets the ring surface making zero angle of contact (16) as assumed. Cram and Haynes (9) show from approximate calculations that the effect of a low contact angle on the surface and interfacial tension measurements is probably small (less than 1% for contact angles up to 10°), but the effect sharply increases as the contact angle becomes larger. We believe that extension of the sphere method of measuring surface and interfacial tensions (7) may resolve this difficulty. One quick way of knowing whether or not the ring surface is completely wetted by one of the liquids, would be to displace the ring slowly from the interface into the liquid phase which is believed to wet its surface. If the liquid makes zero angle of contact with the ring surface, no force will be required to detach it from the interface and to bring it into the liquid phase.

Table 6. Comparison of  $f$  with Harkins and Jordan (1) for small  $R^3/V$ 

$R/a$	$R^3/V$	H. J.	Present	% Difference
(a) Interfacial Tension Measurements				
38.72	0.0689	1.449	1.4267	+1.57%
43.04	0.2083	1.134	1.1210	+1.16%
52.45	0.0997	1.352	1.3400	+0.90%
67.17	0.1308	1.283	1.2677	+1.21%
(b) Surface Tension Measurements				
30	0.24	1.056	1.0585	-0.24%
	0.26	1.039	1.0421	-0.30%
40	0.20	1.119	1.1250	-0.53%
	0.24	1.078	1.0845	-0.60%

Another source of error when an interfacial tension is measured by the ring method is the size of the vessel containing the test liquids. As the small  $R^3/V$  signifies a large interfacial deformation for a given ring, a large vessel is accordingly required, to guarantee the flat level of the interface at large distance from the ring center. A study of the wall effect similar to the work of van Zeggeren et al. (17) is desirable. When a rough estimate

of  $\gamma_{23}$  is available for a system, the minimum vessel size for a given  $R$  can be approximately calculated from figs. 3 and 5(b). From  $\bar{R}$ ,  $R^3/V$  is read using fig. 3; from  $R^3/V$ ,  $\beta_2$  is read using fig. 5(b). Since  $\beta_2$  is defined (12) as the dimensionless radial distance  $\bar{r}_2$  where the outer meniscus assumes the slope angle of  $\phi_2 = 359.5^\circ$  (or  $0.5^\circ$ ), if we can be certain that the interface is flat at  $\bar{r} = \beta_2$ , we may safely say that the effect of the finite size of the vessel is negligible. Therefore, we may say that the minimum radius of the vessel should be at least  $\beta_2/\sqrt{C_{23}}$  and the interface there should be flat. We suspect that the low values of  $f$  obtained by Harkins and Jordan (1) resulted from using too small a container. Formation of the interface concave toward the phase into which the ring is pulled, will result in the force measurement higher, and the value of  $f$  lower than the correct one (18).

A minor error may also be introduced due to the welding of the ring to the support wire connecting it to the balance. Fig. 6(a) shows that, for small  $R^3/V$ , the contact line circle for the inner meniscus stays near the top portion of the ring wire. This will permit the inner meniscus to creep up the surface of the support wire, as shown schematically in fig. 10. Along the portion of the contact line which creeps up the support wire, the interfacial tension pull is practically vertical since the liquid wets the wire; while along the remaining portion on the ring wire, the vertical component is small, e.g.,  $\sin \psi_1 = \sin 190^\circ = -0.174$  for  $R^3/V = 0.027$ , as we can calculate from fig. 6(a). Since the support wire usually has the same radius as the ring wire, the length of such distortion

would be about  $4\alpha$  out of the total length of the contact line of about  $4\pi R$ . This error can be eliminated by choosing a ring made of a thick wire but with thin support wires.

Since the equilibrium of ring at the interface may be maintained beyond the position of maximum force (fig. 2), it will be of interest to know the force at the moment the ring detaches from the interface. Its precise determination however appears to be a difficult task: if the ring is completely free to move, we expect the maximum force to be the detachment force; if the ring is held fixed at each moment as it is slowly raised, it may be the force when the inner and outer menisci approach and touch, although this should be confirmed experimentally. In practice, the ring is neither completely free to move, nor held fixed in space: beyond the position of the maximum force, the ring will probably move sufficiently fast that true static equilibrium never exists. The rupture of the thin film between the inner and outer menisci may also occur before they touch; at the other limit, the viscous thinning of the film may be slow enough to delay rupture (14).

If the ring is not horizontal, additional errors will be introduced. This may be avoided experimentally by employing a flexible support. When the ring is slightly tilted, we may then determine, modifying the derivation made in the earlier work (5), whether or not the torque accordingly produced has the effect of restoring the ring to the horizontal, as we would intuitively expect. For a particular case, Harkins and Jordan (1) showed experimentally that the decrease in the maximum force due to tilting is proportional to the square of the angle of tilt. This aspect of the problem warrants further theoretical study by those interested in precision absolute ring tensiometry.

#### Acknowledgement

The authors are grateful to A. Mar for preparing fig. 2 and providing many helpful suggestions, and to one of the referees who pointed out that the detachment of the ring can occur by the rupture of the film intervening the inner and outer menisci. This research was supported by the Defence Research Board Grant No. 9530-47.

#### Summary

The Harkins-Jordan correction factors which make the ring method an accurate and absolute method of

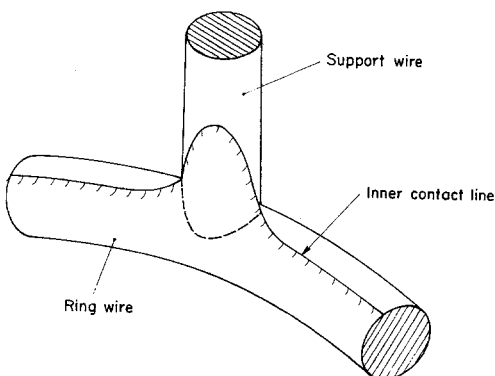


Fig. 10. Creeping-up of the inner meniscus along the surface of the support wire, when  $R^3/V$  is small

measuring surface and interfacial tensions, are calculated theoretically and made available in a tabulated form. The applicable range of the numerical tabulation far exceeds the range of those available in the literature which have been obtained experimentally. With the tabulation, the ring method may be used to measure the interfacial tensions of liquid systems in which the density difference across the interface is very small and the interfacial tension is large, or in which the density difference is large and the tension is small. The theoretical calculations also provide information on the state of the ring at the liquid interface which may be used to increase accuracy of the ring method.

#### Zusammenfassung

Die *Harkins-Jordan* Korrektionsfaktoren, die die Ringmethode als eine genaue und absolute Methode zur Bestimmung von Oberflächen- und Grenzflächenspannungen möglich machen, sind theoretisch berechnet und tabuliert worden. Der anwendbare Bereich dieser numerischen Tafeln überschreitet bei weitem den Bereich jener, die in der Literatur vor vorhanden und experimentell bestimmt worden sind. Mit diesen Tafeln kann man die Ringmethode anwenden für die Grenzflächenspannungsmessungen flüssiger Systeme, in denen der Dichteunterschied beiderseits der Grenzfläche sehr gering und die Grenzflächenspannung sehr groß ist, oder in denen der Dichteunterschied groß und die Spannung klein ist. Die theoretischen Berechnungen darüber hinaus informieren über die Lage des Rings an der flüssigen Grenzfläche, woraus eine erhöhte Genauigkeit der Ringmethode abgeleitet werden kann.

#### References

- 1) *Harkins, W. D.* and *H. F. Jordan*, J. Amer. Chem. Soc. **52**, 1751 (1930).
- 2) *Freud, B. B.* and *H. Z. Freud*, J. Amer. Chem. Soc. **52**, 1772 (1930).
- 3) *Fox, H. W.* and *C. H. Chrisman, Jr.*, J. Phys. Chem. **56**, 284 (1952).
- 4) *Zuidema, H. H.* and *G. W. Waters*, Ind. Eng. Chem. (Anal.) **13**, 312 (1941).
- 5) *Hub, C.* and *S. G. Mason*, J. Colloid Interface Sci. **47**, 271 (1974).
- 6) *Cini, R., G. Loglio* and *A. Ficalbi*, J. Colloid Interface Sci. **41**, 287 (1972).
- 7) *Mar, A.* and *S. G. Mason*, forthcoming publication.
- 8) *Princen, H. M.* and *S. G. Mason*, J. Colloid Interface Sci. **20**, 246 (1965).
- 9) *Cram, P. J.* and *J. M. Haynes*, J. Colloid Interface Sci. **35**, 706 (1971).
- 10) *Princen, H. M.*, in: *E. Matijevic* (Ed.), Surface and Colloid Science, Vol. 2, 1 (New York 1969).
- 11) *Bashforth, F.* and *J. C. Adams*, An Attempt to Test the Theories of Capillary Action, (Cambridge, 1883).
- 12) *Hub, C.* and *L. E. Scriven*, J. Colloid Interface Sci. **30**, 323 (1969).
- 13) *Hub, C.*, Ph. D. Thesis, University of Minnesota, Minneapolis, Minn. (1969).
- 14) *Princen, H. M.* and *E. D. Goddard*, J. Colloid Interface Sci. **38**, 523 (1972).
- 15) *Lord Rayleigh*, Proc. Roy. Soc. (London) **A92**, 184 (1915).
- 16) *Krynnitsky, J. A.* and *W. D. Garrett*, J. Colloid Sci. **18**, 893 (1963).
- 17) *van Zeggeren, F., C. d. Courval* and *E. D. Goddard*, Canad. J. Chem. **37**, 1937 (1959).
- 18) *Mar, A., C. Hub* and *S. G. Mason*, forthcoming publication.

#### Author's address:

Dr. S. G. Mason  
Dept of Chemistry, McGill University  
P.O. Box 6070  
Montreal 101, Quebec (Canada)